Influence of the LPM effect and dielectric suppression on particle air showers

A. N. Cillis, H. Fanchiotti, C. A. García Canal and S. J. Sciutto

Laboratorio de Física Teórica
Departamento de Física
Universidad Nacional de La Plata
C. C. 67 - 1900 La Plata
Argentina
e-mail: cillis@venus.fisica.unlp.edu.ar

Abstract

An analysis of the influence of the Landau-Migdal-Pomeranchuk (LPM) effect on the development of air showers initiated by astroparticles is presented. The theory of Migdal is studied and compared with other theoretical methods. By means of computer simulations and using algorithms that emulate Migdal's theory, including also the so-called dielectric suppression, we study the behavior of the relevant observables in the case of ultra-high energy primaries. We find that the LPM effect can significantly modify the development of high energy electromagnetic showers in certain cases.

PACS numbers: 96.40.Pq, 13.10.+q, 02.70.Lq

1 Introduction

The study of atmospheric showers initiated by high energy astroparticles plays a central role in contemporary cosmic ray physics [1]. The most important component, in number of particles, of the air shower is by far the electromagnetic one. Additionally, many shower observables that give direct information about the properties of the primary depend strongly on its behavior.

Electron bremsstrahlung and pair production are the dominant processes in the electromagnetic shower at very high energies. The standard description of these processes, i.e., the Bethe-Heitler equation [2], can be incomplete at very high energies due to some effects that drastically reduce the corresponding cross sections [3]. Those mechanisms play a relevant role in the development of air showers because they can lengthen them, and consequently move the position of the shower maximum deeper into the atmosphere.

In the present work we study two of the several suppression processes that can affect the high energy electromagnetic interactions [3], namely, the Landau-Pomeranchuk-Migdal (LPM) effect [4, 5] and the dielectric suppression [5, 6]. The first of these effects is due to the multiple scattering while the second one is due to the interaction of the bremsstrahlung photons with the atomic electrons in the medium, through forward Compton scattering.

The LPM effect was studied semi-classically by Landau and Pomeranchuk [4] and the first quantum mechanical approach was given by Migdal [5]. Recently, the experimental confirmation of the LPM effect at the Stanford Linear Accelerator Center (SLAC) [3, 7] has originated new theoretical works [8, 9, 10, 11] and several analysis of its consequences, particularly in cosmic ray physics [12].

The main purpose of our work is the study of the modifications in the development of the air showers that take place when the LPM effect and the dielectric suppression are taken into account. In order to do that we first study the different theoretical approaches of the LPM effect. In particular, we compare the Migdal formulation [5] with other approaches that were developed more recently [3, 8]. We also analyze the modifications of the bremsstrahlung and pair production probabilities in the case of our interest, that is, when the medium is a "layer" of air of infinite thickness and variable density. Our study is, therefore, complementary to the recently published review by Klein [3] which primarily treats the LPM effect in the case of solid targets of finite size, like the ones used in the already mentioned SLAC [7] experiment.

To complete our study we have developed new LPM/dielectric suppression procedures, and we have installed them in the AIRES air shower simulation system [13]. The AIRES code has then been used as a realistic air shower simulator to generate the data used to make our analysis of the influence of the LPM effect on high energy showers.

It is worthwhile to mention that AIRES represents a set of programs to simulate atmospheric air showers and to manage all the associated output data. Most of the physical algorithms of the AIRES system are based on the realistic procedures of the

well-known MOCCA program [14]. AIRES provides some additional features, for example: The Earth's curvature is taken into account allowing safe operation of all zenith angles; the simulation programs can be linked to different alternative hadronic collision models like QGSJET [15] or SIBYLL [16, 17]; etc.

This paper is organized as follows: In section 2 we introduce the different approaches to the LPM effect and compare the Migdal formulation with other ones. In section 3 we explain the practical implementation of the LPM effect and the dielectric suppression into the AIRES program. In section 4 we analyze the results of the air showers simulations performed with such code. Finally, in section 5 we place our conclusions and comments.

2 Theory of the LPM effect

The so-called LPM effect takes place when an ultra-relativistic particle emits low energy bremsstrahlung photons passing through matter. In this case, fewer photons are emitted than predicted for the case of isolated atoms [2]. In a similar way, the cross section for electron-positron pair production is reduced in the case of high energy gamma rays passing through matter.

This effect was first predicted by Landau and Pomeranchuk [4] some 40 years ago. They treated the classical radiation of a high-energy particle in a fluctuating random field inside an infinitely thick medium. Afterwards, Migdal [5] provided the corresponding quantum mechanical theory giving analytical expressions for the bremsstrahlung and pair production cross sections when matter is present. Migdal theory was developed for an infinite target thickness. More recently, an experiment performed at SLAC [7] measured the LPM effect finding that there is an acceptable agreement between the experimental data and Migdal theory which is presently considered the standard treatment.

The experimental confirmation of the LPM effect triggered new theoretical works [8, 9, 10, 11]. In particular, Blankenbecler and Drell [8] and Klein [3] have reanalyzed the problem, upon better approximations than in the earlier works, and they were able to consider effects of finite target thickness. We include in this paper a comparative analysis between different approaches.

To make our paper self-consistent, we include first a qualitative description of the LPM effect explaining the main features of Migdal theory. We then compare the final Migdal results with those of Blankenbecler and Drell.

2.1 Bremsstrahlung

Let us consider first the case of bremsstrahlung where an electron or positron of energy E and mass m emits a photon of energy k in the vicinity of a nucleus of charge Z.

Neglecting the photon emission angle and the scattering of the electron, the minimal

longitudinal momentum transfer[1] to a nucleus, $q_\parallel$, in the case when $E \gg k$ and $E \gg mc^2$, is given by [3]

$$q_\parallel = \frac{km^2c^3}{2E(E-k)}. \tag{1}$$

The formation length can be defined according to the uncertainty principle: $l_{fo} = \hbar/q_\parallel$. l_{fo} is the distance over which the interaction amplitudes can add coherently. It is straightforward to show [3] that if other interactions are present while the electron is traversing this distance, then the resulting amplitude will, in general, be reduced.

Let us consider the case when multiple scattering takes place during the radiation emission process. Using a small angle approximation, the longitudinal momentum transfer can be expressed as

$$q_\parallel = \frac{km^2c^3}{2E(E-k)} + \frac{k\theta_{MS/2}^2}{2c} \tag{2}$$

where $\theta_{MS/2}$ is the multiple scattering angle in half the formation length, that is $(E_s/E)\sqrt{l_f/(2X_0)}$, with $E_s = mc^2\sqrt{4\pi/\alpha} = 21.2$ MeV ($\alpha \approx 137^{-1}$, is the fine structure constant), and $X_0 = \left[4\eta\alpha r_e^2 Z^2 \ln(184Z^{-1/3})\right]^{-1}$ is the radiation length ($r_e = e^2/mc^2$ is the classical electron radius, and η is the number of atoms per volume unit). The effect of multiple scattering becomes significant when the second term of equation (2) is comparable in magnitude with the first one. This is the case when

$$E\left[\frac{1-y}{y}\right] \gtrsim E_{\rm LPM} \tag{3}$$

where

$$y = \frac{k}{E}, \tag{4}$$

and

$$E_{\rm LPM} = \frac{m^4c^7X_0}{\hbar E_s^2} \tag{5}$$

is a characteristic, material dependent, energy which gives the scale where the effect cannot be neglected. For a given energy E, the emission of photons with

$$y \lesssim \frac{E}{E + E_{\rm LPM}} \tag{6}$$

will be affected by the interference due to multiple scattering; and this implies that for $E \gg E_{\rm LPM}$ the effect extends to the entire photon spectrum $0 < y < 1$.

The characteristic energy $E_{\rm LPM}$ can be expressed as

$$E_{\rm LPM} = \frac{m^2c^3}{16\pi\hbar\eta r_e^2 Z^2 \ln(184Z^{-1/3})}. \tag{7}$$

[1]The minimal longitudinal momentum transfered to the nucleus occurs when the final electron and the photon follow in the same direction of motion than the initial electron.

This equation makes evident the fact that $E_{\rm LPM}$ diminishes when the density of the medium increases. Therefore, for dilute media, the LPM effect will be appreciable only for energies much higher than the typical ones used in experiments with dense targets [3, 7]. In fact, for air in normal conditions $E_{\rm LPM} \cong 2.2 \times 10^8$ GeV; one can compare this energy with the energy of the electron beam of 8 and 25 GeV used at SLAC [3, 7].

The formation length, when multiple scattering is considered, can be put in the form

$$l_f = l_{fo}\left[1 + \frac{m^2 c^3 l_f}{2\hbar E_{\rm LPM}}\right]^{-1}. \tag{8}$$

When multiple scattering is the dominating process, it turns into

$$l_f = l_{fo}\sqrt{\frac{kE_{\rm LPM}}{E(E-k)}}, \tag{9}$$

To measure the strength of the effect it is convenient to introduce the suppression factor through

$$S = \frac{d\sigma_{\rm LPM}/dk}{d\sigma_{BH}/dk} \tag{10}$$

where $d\sigma_{BH}/dk$ stands for the bremsstrahlung cross section given by the classical theory of Bethe and Heitler [2].

The fact that the cross sections are proportional to the formation length gives rise to

$$S \cong \sqrt{\frac{kE_{\rm LPM}}{E(E-k)}} \tag{11}$$

For k small in comparison with E, The cross section found by Bethe and Heitler [2] is proportional to $1/k$. If multiple scattering is taken into account, this proportionality changes, due to equation (11), to $1/\sqrt{k}$.

In the Migdal theory of the LPM effect [5], the multiple scattering is treated as a diffusion mechanism. The average radiation per collision and the interference between the radiation from different collisions are then computed. When collisions occur too close together, destructive interference reduces the radiation. The multiple scattering is treated using the Fokker-Planck technique to solve the corresponding Boltzmann transport equation. Migdal includes quantum effects, such as electron spin and photon polarization, but his calculations only apply for a target of infinite thickness. The resulting cross section for the bremsstrahlung process reads:

$$\frac{d\sigma_{\rm LPM}}{dk} = \frac{4\alpha r_e^2 \xi(s)}{3k}\{y^2 G(s) + 2[1+(1-y)^2]\Phi(s)\} Z^2 \ln\left(\frac{184}{Z^{\frac{1}{3}}}\right) \tag{12}$$

where

$$s = \sqrt{\frac{kE_{\rm LPM}}{8E(E-k)\xi(s)}}, \tag{13}$$

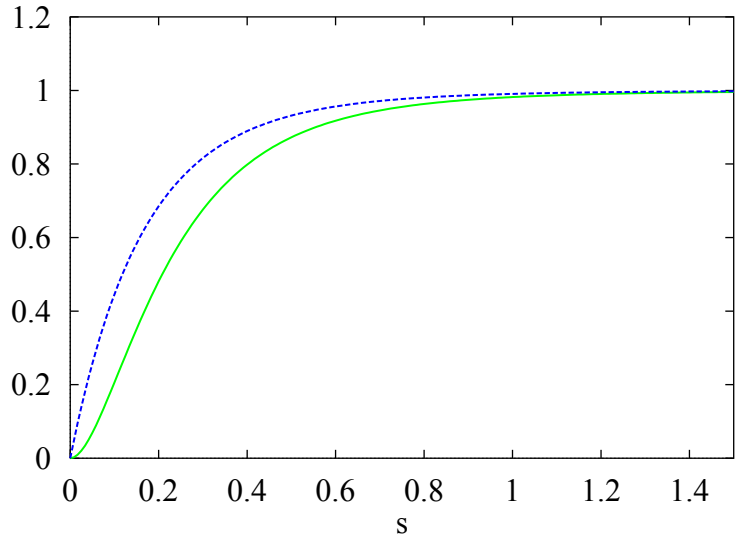

Figure 1. Functions $G(s)$ (solid line) and $\Phi(s)$ (dashed line), appearing in Migdal theory.

$$\xi(s) = \begin{cases} 2 & \text{if } s \leq s_1 \\ 1 + \ln s / \ln s_1 & \text{if } s_1 < s < 1, \\ 1 & \text{if } s \geq 1 \end{cases} \tag{14}$$

($\sqrt{s_1} = Z^{1/3}/184$) and

$$G(s) = 48s^2 \left(\frac{\pi}{4} - \frac{1}{2} \int_0^\infty e^{-st} \frac{\sin(st)}{\sinh(t/2)} dt \right), \tag{15}$$

$$\Phi(s) = 12s^2 \left(\int_0^\infty e^{-st} \coth(t/2) \sin(st) dt \right) - 6\pi s^2. \tag{16}$$

The functions $G(s)$ and $\Phi(s)$ are plotted in figure 1. These plots show clearly that both $G(s)$ and $\Phi(s)$ belong to the interval $[0, 1]$ for all $s \geq 0$ and that their limits for s going to zero (infinity) are 0 (1). It can also be shown [5] that for $s \ll 1$, these functions can be approximated through

$$G(s) \cong 12\pi s^2, \tag{17}$$

$$\Phi(s) \cong 6s(1 - \pi s). \tag{18}$$

Therefore, when $s \ll 1$ the suppression is important (the cross section is reduced, $S \ll 1$), while for $s \gg 1$ there is no suppression ($S \cong 1$) and the Migdal cross section reproduces the main terms of the Bethe-Heitler equation [2] if complete screening is

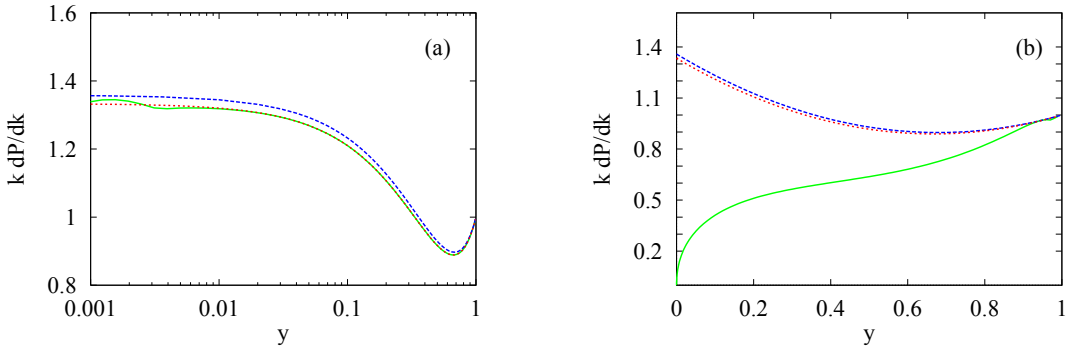

Figure 2. Comparison between Migdal and Bethe-Heitler theories. Migdal theory (solid line), Bethe-Heitler theory (dashed line) and no suppression limits of the Migdal theory (dotted line). The electron energies are (a) $E = 10^{14}$ eV and (b) $E = 10^{18}$ eV, and the medium is air at vertical depth of $X_v = 1000$ g/cm^2 ($\rho = 1.19$ kg/m^3).

considered, namely

$$\frac{d\sigma_0}{dk} = \frac{4\alpha r_e^2}{3k}\{y^2 + 2[1 + (1-y)^2]\}Z^2 \ln\left(\frac{184}{Z^{\frac{1}{3}}}\right). \tag{19}$$

In figure 2, the results coming from Migdal theory (12), from its no suppression limit (19) and from the screened[2] Bethe-Heitler equation [2] are compared for electron energies of 100 TeV and 1 EeV (10^{18} eV). The medium is air[3] at the altitude h which corresponds to a vertical depth $X_v = 1000$ g/cm^2 ($X_v(h) = \int_h^\infty \rho(z)dz$ [13], $X_v(0) \cong 1000$ g/cm^2, $X_v(100\text{ km}) \cong 0$); at this altitude the density is $\rho = 1.19$ kg/m^3. In figure 2a, which corresponds to an electron energy of 100 TeV, the Bethe-Heitler theory and the $s \gg 1$ limit of Migdal theory agree within the 2.5% relative error level. In concordance with equation (6) the region of photon spectrum where the LPM suppression is significant grows when the primary energy is enlarged, and affects virtually the complete range $0 < y < 1$ when the energy of the electron is 10^{18} eV (in this case $E_{\text{LPM}} \cong 2.8 \times 10^{17}$ eV $= 280$ PeV). Notice also that the quantity presented in figure 2 is kdP/dk where dP/dk is the probability of emission of a bremsstrahlung photon with energy in the interval $[k, k + dk]$, in a distance of one radiation length. dP/dk is related to the cross section via

$$\frac{dP}{dk} = \eta X_o \frac{d\sigma}{dk} \tag{20}$$

[2]The screening effect of the outer electrons has been calculated by Bethe and Heitler on the basis of the Fermi-Thomas model of the atom. The influence of the screening on a radiation process is determined by the quantity $\gamma = 100(m/E)[y/(1-y)]Z^{-1/3}$. For $\gamma \gg 1$ screening can be practically neglected while one has complete screening for $\gamma \cong 0$ [2, 18].

[3]For altitudes up to 90 km above see level, the air is a mixture of 78.09% N_2, 20.95% O_2 and 0.96% other gases [19] which can be adequately modeled as an homogeneous substance with atomic charge and mass numbers $Z_{\text{eff}} = 7.3$ and $A_{\text{eff}} = 2 \times Z_{\text{eff}}$, respectively.

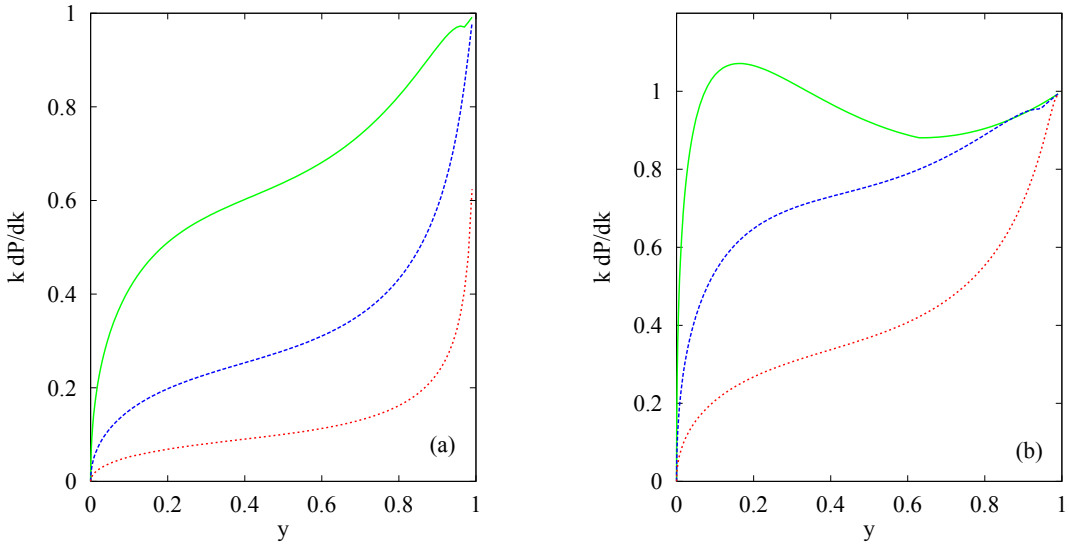

Figure 3. Bremsstrahlung probability according to Migdal theory (kdP/dk). The electron energies are $E = 10^{20}$ eV (solid line), $E = 10^{19}$ eV (dashed line) and $E = 10^{18}$ eV (dotted line). The medium is air at the vertical depth of $X_v = 1000$ g/cm^2 ($\rho = 1.19$ kg/m^3) (a), and $X_v = 50$ g/cm^2 ($\rho = 78$ g/m^3) (b).

The plots in figure 3 illustrate the dependence of the LPM effect with the density of the medium. In this figure the probability (20) is plotted versus y for several electron energies. The medium is air at two representative altitudes: (a) Vertical atmospheric depth $X_v = 1000$ g/cm^2, which corresponds approximately to an altitude of 300 m.a.s.l ($\rho = 1.19$ kg/m^3, $E_{\rm LPM} \cong 280$ PeV); (b) $X_v = 50$ g/cm^2, which corresponds approximately to 20,000 m.a.s.l ($\rho = 78$ g/m^3, $E_{\rm LPM} \cong 5.78$ EeV). The plots in figure 3a show that an important suppression takes place at all the energies considered and becomes severe for the 10^{20} eV case. Notice that the curve for 10^{18} eV is also plotted in figure 2b. On the other hand, the LPM effect does not seriously affect the bremsstrahlung probabilities for 10^{18} eV electrons at $X_v = 50$ g/cm^2 as shown in figure 3b. In this case the critical energy where the effect becomes significant is placed around 10^{19} eV since $E_{\rm LPM}$ is some 20 times larger than the corresponding value for figure 3a.

When the effect of the polarization of the medium is taken into account, a significant alteration in the bremsstrahlung formula for soft photons appears. The interaction of a photon with the atomic electrons produces another kind of suppression of the cross section that is called *dielectric suppression* [5, 6]. If we take into consideration that the dielectric constant of the medium is different from one, i.e., $\varepsilon = 1 - (\hbar\omega_p)^2/k^2$, where ω_p is the well-known plasma frequency ($\omega_p^2 = 4\pi Ze^2\eta/m$; for air in normal conditions $\hbar\omega_p = 0.73$ eV), then the longitudinal momentum transferred to a nucleus changes

from equation (1) to

$$q_{\parallel} = \frac{km^2c^3}{2E(E-k)} + \frac{(\hbar\omega_p)^2}{2ck}. \tag{21}$$

Consequently, when the second term in the last equation is comparable with the first, the dielectric suppression becomes important. This happens when the energy of the photon is much lower than a critical energy given by $k_{\rm crit} = \hbar\omega_{\rm crit}$ with

$$\omega_{\rm crit} = \omega_p \sqrt{\frac{E(E-k)}{m^2c^4}} \cong \omega_p \frac{E}{mc^2} \tag{22}$$

It is worth to notice that the correction due to the dielectric constant is certainly negligible for the propagation phenomenon. On the contrary, in our case of the emission process, the effect is measurable because here the scale fixing parameter is the critical frequency given by equation (22), and not the plasma frequency. Notice also that this critical frequency is exactly the plasma frequency when measured in the electron rest frame. If we define now

$$y_{\rm diel} = \frac{\hbar\omega_p}{mc^2}, \tag{23}$$

equations (21) and (22) tell us that the dielectric suppression takes place when $y \ll y_{\rm diel}$.

The Migdal approach takes into account this dielectric effect. Since dielectric suppression occurs for $y \ll y_{\rm diel} \ll 1$, the term in $G(s)$ can be neglected. In that case, the cross section becomes [5]

$$\frac{d\sigma_{\rm LPM}}{dk} = \frac{16\alpha r_e^2 \xi(s)}{3k\delta} \Phi(s\delta) Z^2 \ln\left(\frac{184}{Z^{\frac{1}{3}}}\right), \tag{24}$$

where $\delta = 1 + (y_{\rm diel}/y)^2$.

Figure 3 illustrates the influence of the dielectric suppression on the bremsstrahlung cross section (24) where the probability for bremsstrahlung is plotted against y in the case of $E = 10^{18}$ eV. The emission probability is suppressed for $y \leq y_{\rm diel} \cong 10^{-8}$. This corresponds to photon energies $k < 10$ GeV.

2.2 Pair production

The pair production process can be treated similarly as bremsstrahlung. The corresponding expression for the cross section of this interaction, where a photon of energy k produces a pair e^+e^- of energies E and $k-E$ respectively, can be obtained immediately from the bremsstrahlung formula [3, 5]. In this case the cross section reads

$$\frac{d\sigma_{\rm LPM}(\gamma \to e^+e^-)}{dE} = \frac{4\alpha r_e^2 \xi(\widetilde{s})}{3k} \{G(\widetilde{s}) + 2[u + (1-u)^2]\Phi(\widetilde{s})\} Z^2 \ln\left(\frac{184}{Z^{\frac{1}{3}}}\right) \tag{25}$$

where

$$u = \frac{E}{k} \tag{26}$$

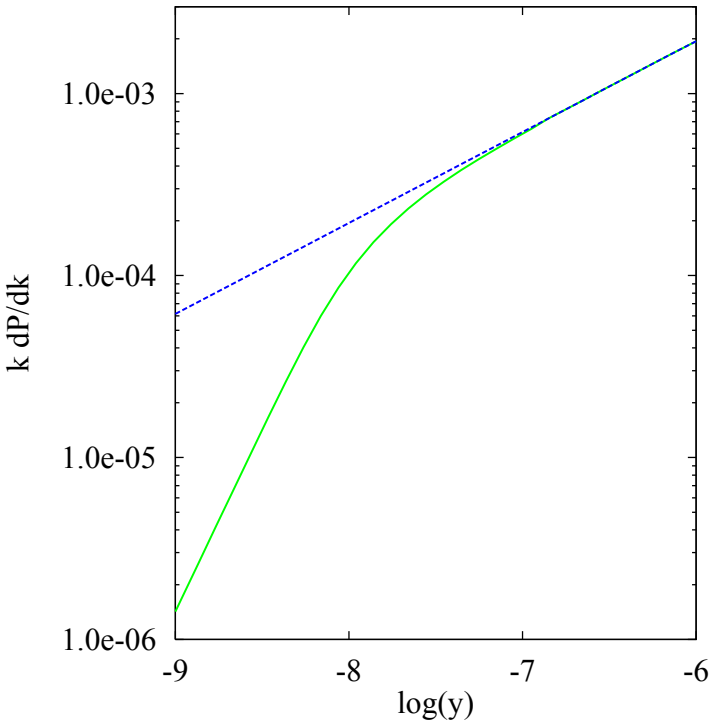

Figure 4. Bremsstrahlung probability according to Migdal theory (kdP/dk). The probabilities taking (solid line) and not taking (dashed line) into account the influence of dielectric suppression are plotted versus $log_{10}y$. The energy of the electron is 10^{18} eV and the medium is air at a vertical depth $X_v = 1000$ g/cm^2 ($\rho = 1.19$ kg/m^3).

and

$$\widetilde{s} = \sqrt{\frac{kE_{\rm LPM}}{8E(k-E)\xi(\widetilde{s})}} \tag{27}$$

Clearly the dielectric suppression on the cross section of the electron-positron pair production can always be neglected. This follows from the fact that the polarization of the medium influences only the soft photons whose energies are much smaller than that of the electrons [6].

Figure 5 shows the normalized probability of pair production at atmospheric depths of 1000 g/cm^2 (a) and 50 g/cm^2 (b) for different energies of the primary photon. The production probabilities are progressively suppressed when the primary energy rises. From figure 5, it is also evident that symmetric processes ($u \sim 0.5$) are the most affected by the LPM suppression.

2.3 Comparison with other approaches to the LPM effect

We should remember that the Migdal approach does not include all the corrections that should in principle be included. In fact, the inelastic form factor that accounts for inelastic interactions with the atomic electrons, and the term that accounts for the Coulomb corrections because the interaction takes place with the electron in the Coulomb field of the nucleus [20, 21] are not taken into account. However, Migdal formulation proves to work sufficiently well when its results are compared with exper-

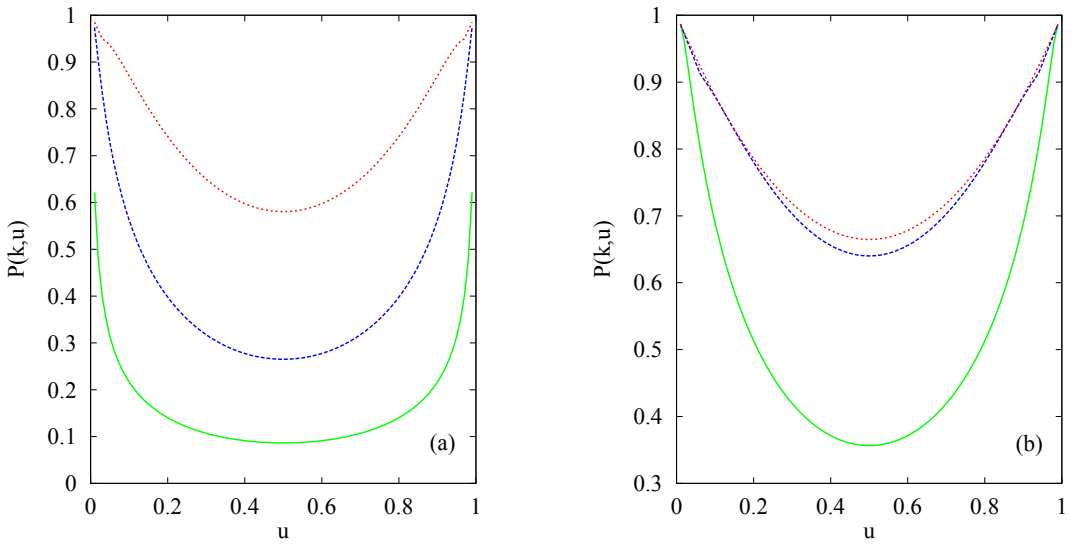

Figure 5. Pair production probability, $P(k,u)$, according to Migdal theory plotted versus u for different values of the photon energy: 10^{20} eV (solid line), 10^{19} eV (dashed line) and 10^{18} eV (dotted line). The medium is air at the vertical depth of $X_v = 1000$ g/cm^2 ($\rho = 1.19$ kg/m^3) (a), and $X_v = 50$ g/cm^2 ($\rho = 78$ g/m^3) (b).

imental data [7].

Blankenbecler and Drell [8] have computed, in an alternative way, the magnitude of the LPM suppression. They have used the eikonal formalism, standard in the study of scattering from an extended target. This approach leads to a physically clear quantum-mechanical treatment of multiple scattering and from that to the derivation of the LPM suppression of soft photon radiation from high energy electrons in matter. The approach includes as limiting cases the Bethe-Heitler [2] radiation from a charged particle scattering against an isolated atom, relevant for a thin target and, in the opposite limit, the LPM effect which suppresses the radiation in a thick target. Their result for thick targets reads

$$k\frac{dP}{dk} = \frac{2\alpha y m^2 c^2 \ell}{\pi E \hbar}(I_1 - I_2) \tag{28}$$

where ℓ is the target thickness and

$$I_1 = w\int_0^\infty \frac{2 + 3r(\sqrt{1+4wx}-1)}{1+4wx-\sqrt{1+4wx}}\sin x\, dx, \tag{29}$$

$$I_2 = \int_0^\infty \frac{\sin x}{x}\, dx = \frac{\pi}{2} \tag{30}$$

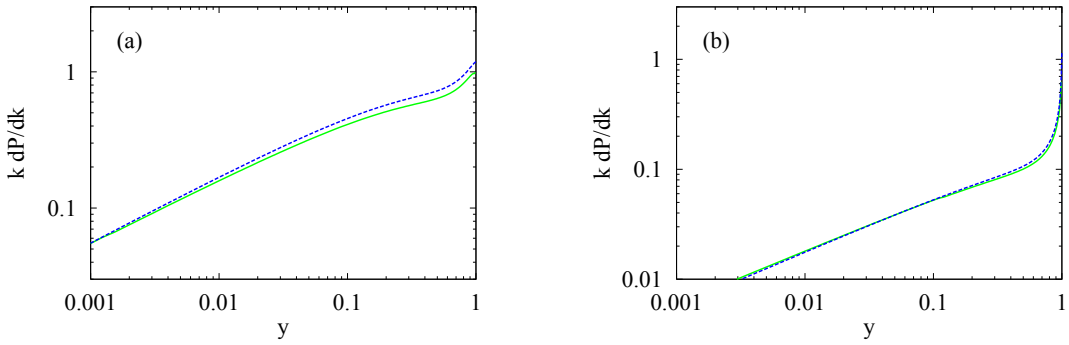

Figure 6. Comparison between Migdal theory (solid line) and Blankenbecler and Drell formulation (dashed line). The electron energies are 10^{18} eV (a) and 10^{20} eV (b). The medium is air and the vertical depth is $X_v = 1000$ g/cm^2 ($\rho = 1.19$ kg/m^3).

where

$$r = \frac{1+(1-y)^2}{2(1-y)}, \tag{31}$$

$$w = \frac{E}{6E_{\rm LPM}}\left(\frac{1-y}{y}\right)\frac{\ell}{X_o} \tag{32}$$

The transition to the LPM regime occurs for $w \cong 1$ and the extreme LPM limit for $w \gg 1$ in concordance with the relation (3).

Migdal theory contains a number of approximations that are not very transparent on physical grounds [8]. On the other hand, the Blankenbecler and Drell formulation is theoretically more robust in its principles, but does not include dielectric suppression. Migdal results are simpler to treat numerically and there are no significant differences between the two approaches, as shown in figure 6 where both predictions are plotted for different energies.

To make these plots we have evaluated the integral (29) numerically. Our results can be considered as a generalization of the analysis presented in reference [8] which corresponds to the limiting cases of negligible ($w \ll 1$) or severe ($w \gg 1$) suppression.

In reference [3], other approaches to the LPM effect [9, 10, 11] are reviewed; and similarly as in the case of the Blankenbecler and Drell formulation their results are not in contradiction with Migdal theory. It is worth noticing that the main differences between such different approaches appear when considering finite thickness slabs, which is not the case of interest in our work, devoted to the study of the LPM effect in an infinite dilute medium like the Earth's atmosphere.

3 Practical Implementation

During the computer simulation of a ultra-high energy air shower, the processes of emission of bremsstrahlung photons and e^+e^- pair production need to be calculated some millions of times. This requires that the algorithms used in such calculations should be fast enough to let the simulations complete in a moderate amount of time. The Migdal formulation for bremsstrahlung and pair production can be implemented fulfilling those requirements [14] and, as discussed in the previous section, its results are in acceptable agreement with other alternative approaches. To fix ideas, we shall illustrate the practical implementation in the case of bremsstrahlung; the algorithm for pair production is completely similar.

The probability of equation (20) can be put in the form

$$\frac{dP}{dk} = \frac{dP_0}{dk} F(E,k) \tag{33}$$

where

$$\frac{dP_0}{dk} = \frac{1}{3k} \tag{34}$$

and

$$F(E,k) = \xi(s)\{y^2 G(s) + 2[1+(1-y)^2]\Phi(s)\} \tag{35}$$

s, $\xi(s)$, $G(s)$ and $\Phi(s)$ are defined in equations (13-16). Therefore it is possible to simulate the bremsstrahlung processes in two steps [13, 14]. (i) Rough approach using the probability (34), (ii) Correction to (i) using the rejection approval algorithm to give the exact distribution (33). The correction factor in the function $F(E,k)$ adequately normalized. Step (i) relates with the normal, Bethe-Heitler bremsstrahlung and can be processed straightforwardly. To complete step (ii) it is necessary to evaluate s, $\xi(s)$, $G(s)$ and $\Phi(s)$. s and $\xi(s)$ can be conveniently calculated by means of repeated iterations of equations (13) and (14) starting with the initial value $\xi(s) = 1$. This iterative process normally converges in a single step. The functions $G(s)$ and $\Phi(s)$ can be put in terms of the complex Ψ functions (the logarithmic derivatives of the Γ functions)

$$G(s) = 48s^2 \left\{ \frac{\pi}{4} + \mathrm{Im}\Psi\left(s + \frac{1}{2} + is\right) \right\}, \tag{36}$$

$$\Phi(s) = 12s^2 \left\{ \mathrm{Im}[\Psi(s+is) + \Psi(s+1+is)] - \frac{1}{2} \right\}. \tag{37}$$

These equations allow to obtain accurate estimations for $G(s)$ and $\Phi(s)$ using the standard algorithms to evaluate the complex Ψ function [22], but are not suitable for production procedures which must be fast. In this case it is better to represent $G(s)$

i	a_i	b_i	c_i	d_i
1	–	7.4783	–	5.0616
2	–	30.845	11.158	11.428
3	48.642	50.609	18.557	–
4	110.12	–	–	–

Table 1. The coefficients for the rational expansions of functions G and Φ (equations (38) and (39)).

and $\Phi(s)$ by means of rational functions:

$$G(s) = \frac{12\pi s^2 + a_3 s^3 + a_4 s^4}{1 + b_1 s + b_2 s^2 + b_3 s^3 + a_4 s^4}, \tag{38}$$

$$\Phi(s) = \frac{6s + c_2 s^2 + c_3 s^3}{1 + d_1 s + d_2 s^2 + c_3 s^3} \tag{39}$$

where the coefficients are adjusted to minimize the maximum relative error for $s > 0$. Notice that equations (38) and (39) give exact results for $s = 0$ and $s \to \infty$. The fitted coefficients are listed in table 1; the maximum relative error for $G(s)$ ($\Phi(s)$) is 0.15% (0.12%). The dielectric suppression can be easily implemented as a scaling factor to s, as it clearly follows from equation (24). In AIRES this scaling factor correction is applied when $y_{\rm diel}/y > 1/2$, i.e., the dielectric suppression is neglected in all cases where $y_{\rm diel}/y < 1/2$.

4 Simulations

We have investigated the modifications in the bremsstrahlung and pair production cross sections due to the LPM effect, for individual processes in different conditions. In this section we are going to analyze the influence of the effect in the development of air showers initiated by ultra-high energy astroparticles.

There are two characteristics that must be taken into account when analyzing the shower development:

1. *The atmosphere is inhomogeneous,* the density of the air diminishes six orders of magnitude when the altitude goes from sea level to 100 km [19], and therefore the characteristic energy $E_{\rm LPM}$ of equation (7) varies accordingly. As a result, the suppression in the corresponding cross sections depends strongly on the altitude where they occur. In figure 7 the energy $E_{\rm LPM}$ is plotted against the vertical atmospheric depth, for X_v in the range 1 g/cm^2 (50 km above sea level) to 1000 g/cm^2 (about sea level). To illustrate the meaning of this plot let us consider a ultra-high energy electromagnetic process with a primary energy of, say, $E = 10^{20}$

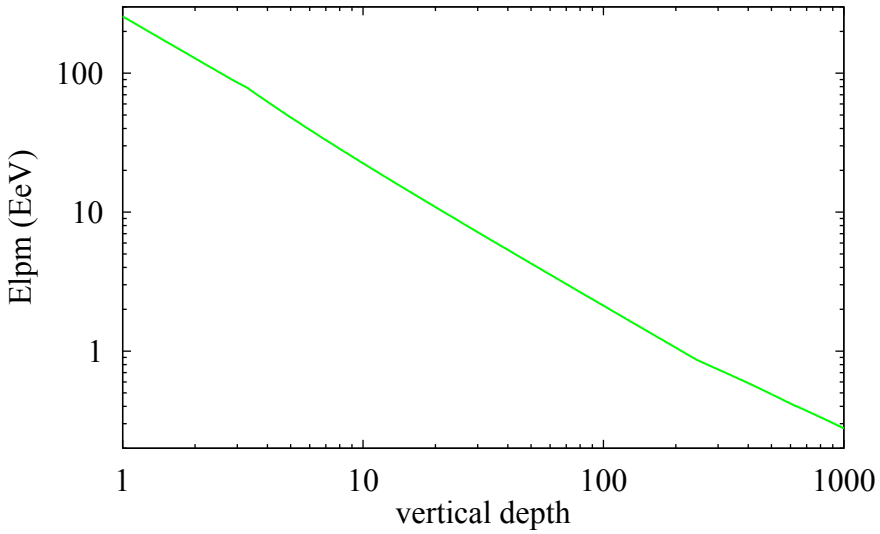

Figure 7. $E_{\rm LPM}$ versus vertical atmospheric depth (in g/cm^2).

eV = 100 EeV: If the primary particle is located at an altitude of 100 g/cm^2 the process will be strongly suppressed whereas if it is located at $X_v < 1$ g/cm^2 the suppression is negligible.

2. *The number of particles in the ultra-high energy showers is very large* (about 10^{11} for a primary energy of 10^{20} eV), and therefore the influence of the LPM effect on *global* observables may not be visible if the fraction of particles affected by the suppression is not large enough.

To estimate how the LPM effect can modify the shower development when the preceding features are taken into account we have run a set of computer simulations using the AIRES program [13] to determine what is the average fraction of electromagnetic particles (gammas, electrons and positrons) significantly affected by the LPM suppression. We have performed simulations using 3×10^{20} eV gamma or proton primaries. The particles were injected at the top of the atmosphere (100 km above sea level) with vertical incidence. In figure 8 the fraction of particles whose energies are greater than $E_{\rm LPM}/4$ is plotted versus the vertical depth. In the case of gamma primaries, the results coming from simulations where the LPM effect is taken into account are plotted (full line) together with similar data obtained without evaluating such effect (dashed line). We can see that in all cases the relative number of particles suffering the LPM effect diminishes when X_v grows, reaching zero for points that are always above 500 g/cm^2. In the case of proton primaries, the electromagnetic shower starts after the first hadronic interactions (mainly after π^0 decays) and so the energies involved are smaller than the primary energy. For this reason, the fraction of LPM particles vanishes faster than in the case of gamma primaries. This corresponds to the dotted line of figure 8,

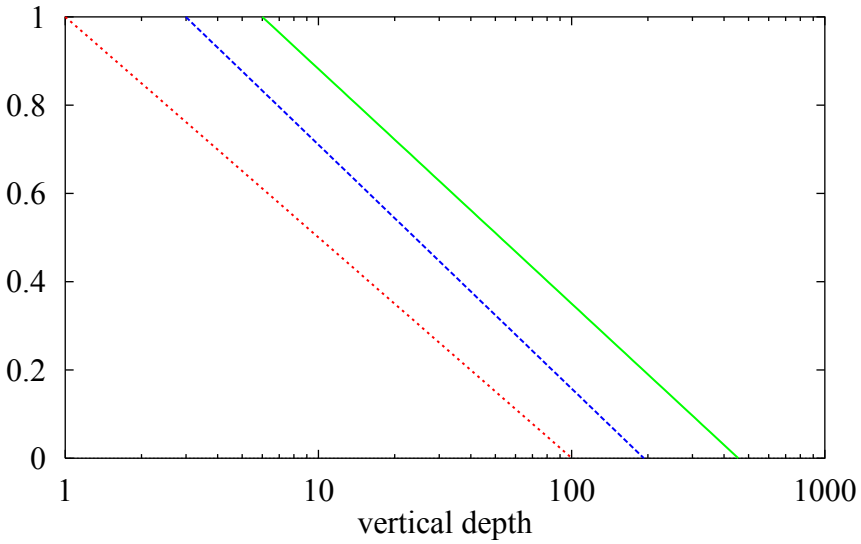

Figure 8. Fraction of air shower particles with energy larger than $E_{\rm LPM}/4$, plotted as a function of the vertical atmospheric depth. The straight lines are fits to simulation data obtained using AIRES, and should be regarded as qualitative indicators. The full (dashed) line correspond to showers initiated by gamma primaries propagated taking (not taking) into account the LPM effect. The dotted line corresponds to a proton primary. In all cases the primary energy is 3×10^{20} eV and the shower axis is vertical.

which reaches zero at $X_v = 100$ g/cm^2.

Of course, the plots represented in figure 8 must be regarded just as qualitative indicators. They are linear fits to averages of many showers with varying starting altitude. Since each shower starts at a different altitude, the fraction of particles capable of undergoing the LPM effect will vary accordingly: If a shower starts very high in the atmosphere, at $X_v < 5$ g/cm^2 for example, it is likely that the LPM effect will not significantly affect its development since the first interactions will take place in a region where $E_{\rm LPM}$ is very high (see figure 7). On the other hand, a penetrating primary particle starting the shower at $X_v > 100$ g/cm^2 will surely show a significant modification in its longitudinal development due to the LPM suppression.

It is worthwhile mentioning that the influence of the LPM effect on the shower development depends also on the inclination of the shower: For large zenith angles it is more probable that the showers will start in points where the density of the air is very low, and so a smaller suppression must be expected in this case.

The most evident signature of the impact of the LPM effect on the shower development is the shift on the position of the shower maximum, $X_{\rm max}$.[4] This can be easily

[4]The shower maximum, $X_{\rm max}$, is defined as the atmospheric depth of the point where the total number of charged particles is maximum. The number of charged particles at $X_{\rm max}$ is noted as $N_{\rm max}$.

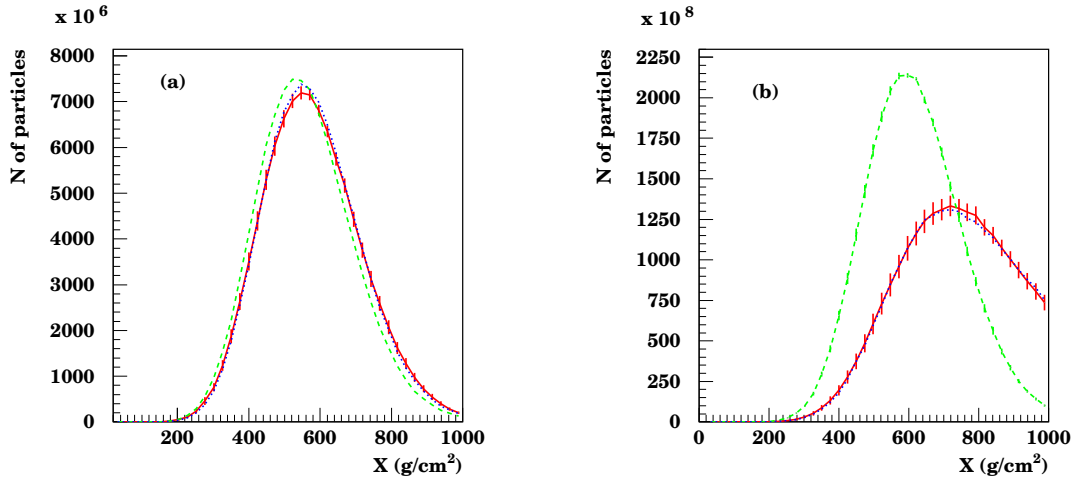

Figure 9. Longitudinal development of charged particles, obtained by means of Monte Carlo simulations using AIRES [13], plotted versus the vertical atmospheric depth. The primary particle is a photon injected at the top of the atmosphere (100 km above sea level) with a zenith angle of 60 degrees. The primary energies are 10^{19} eV (a) and 3×10^{20} eV (b). The solid (dashed) lines correspond to calculations that include (do not include) the LPM effect. The dotted lines correspond to the LPM case but without the dielectric suppression. In some cases the error bars (the RMS errors of the means) were not plotted for clarity; they are, in general, smaller or comparable to the represented ones.

seen in figure 9 where the total number of charged particles for showers initiated by gamma rays is plotted against the vertical depth. These data were obtained by means of computer simulations using the program AIRES [13], and correspond to inclined showers with zenith angle 60 degrees; the primary particles are injected at the top of the atmosphere and the ground level is located at a vertical depth of 1000 g/cm^2. Two primary energies are considered, namely, 10^{19} eV (figure 9a) and 3×10^{20} eV (figure 9b).

The severe suppression suffered by the first interactions that start the shower shows up clearly in figure 9b where the plot corresponding to the simulations performed taking into account the LPM effect shows significantly more penetrating showers that develop deeper in the atmosphere in comparison with the non-LPM ones. The position of $X_{\max}$ is shifted in about 130 g/cm^2 (about 260 g/cm^2 measured along the shower axis) when the LPM procedures are switched on. The number of particles at the maximum, $N_{\max}$ is also affected: It is about a 40% smaller in the LPM suppressed showers. This is mainly due to the fact that the electrons and positrons loss more energy in ionization

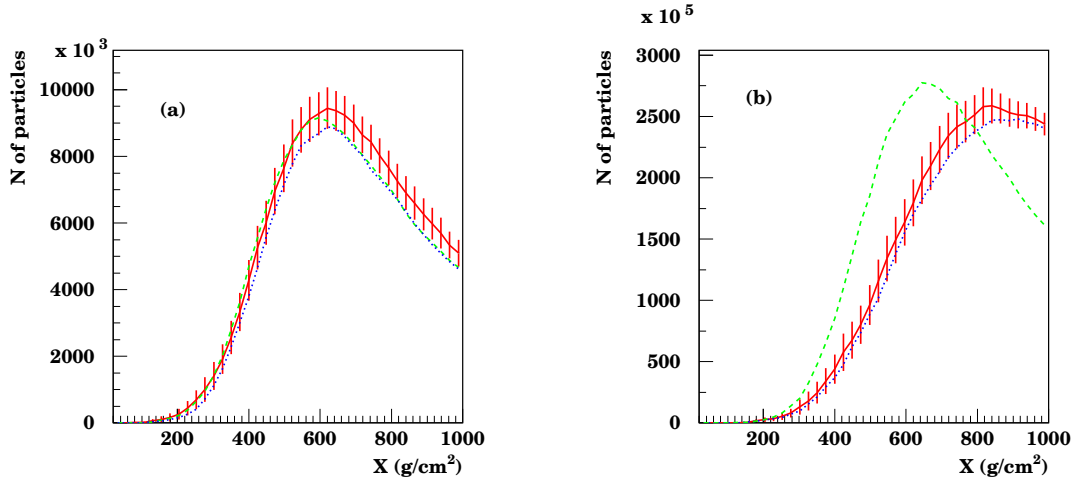

Figure 10. Same as figure 9, but for the longitudinal development of the number of muons.

processes before being able to generate bremsstrahlung photons, and therefore the shower reaches its maximum generating less particles than in the non-LPM case.

For lower primary energies the influence of the LPM effect on the development of the shower is less significant, as shown in figure 9 a for the case of 10^{19} eV gamma showers. Accordingly with the results of our simulations, the LPM effect does not seriously modify the shower longitudinal profile (in the case of gamma primaries) when the primary energy is less than 10^{18} eV.

The longitudinal development of the number of muons is also dependent on the LPM effect as shown in figure 10.

These plots also show the results of simulations made with the LPM effect switched on, but without considering the dielectric suppression. The impact of this last effect is of course less important but no small enough to justify not considering it, and in fact it is more important in relative terms than in the case of the longitudinal development of charged particles (figure 9). It is interesting to describe how the number of muons can be altered when the dielectric suppression of electron bremsstrahlung photons is taken into account: In the case of electrons of energy slightly below the primary energy, that is, about 10^{18} eV, the dielectric suppression diminishes the probability of emission of photons with energies below 10 GeV ($y < y_{\rm diel} \approx 10^{-8}$), producing a relative enlargement of the number of event with photon energies slightly above this limit. Such photons can undergo photonuclear reactions creating pions which in turn may decay into muons; and it is clear that if their number is enlarged so will be the number of secondary muons (compare the full and dotted lines of figure 10b).

If the primary particle is not electromagnetic, the influence of the LPM effect will

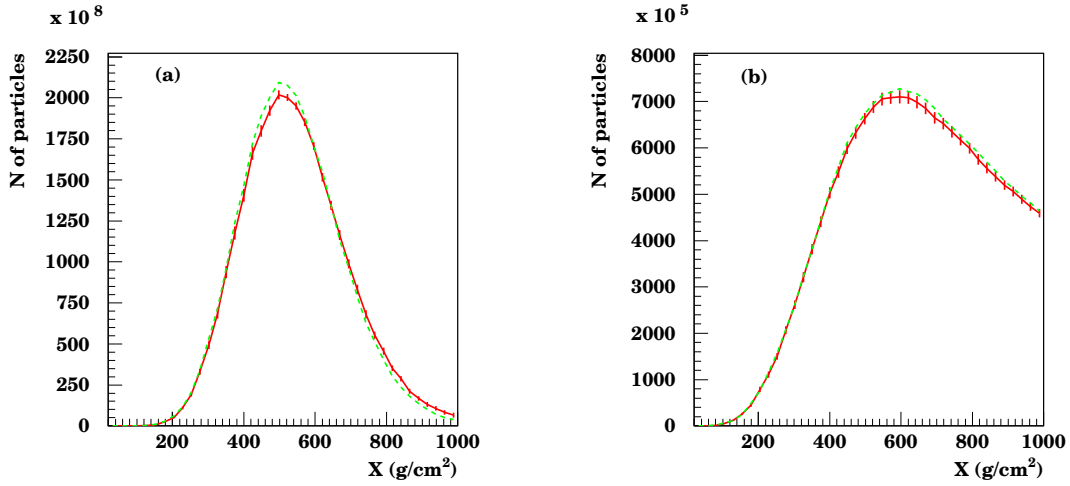

Figure 11. Longitudinal development of charged particles (a) and muons (b) for showers initiated by proton primaries. The shower parameters are as in figure 9.

not depend directly on the primary energy, but on the energy of the particles that initiate the electromagnetic shower. In the case of showers with hadronic primaries, protons for example, the electromagnetic shower is typically started by the gamma rays product of decays of π^0 mesons produced after inelastic hadronic processes that take place when the primary collides against an atmospheric nucleus. For primary energies larger than 10^{19} eV, an inelastic collision hadron-nucleus produces hundreds of secondaries, most of them having energies which are 1 to 4 orders of magnitude smaller than the primary energy. Roughly speaking, this means that the electromagnetic shower maximum energy is 2 or 3 orders of magnitude below the energy of the primary, and accordingly with the data presented in figure 9 this means that the LPM effect will not produce serious distortion in the shower development unless the energy of the primary hadron is well above 10^{21} eV. This agrees with our results presented in figure 11 which correspond to the longitudinal development of 3×10^{20} eV proton showers: The curves corresponding to both LPM "on" and "off" cases do not present significant differences.

Another remarkable feature is the increase of the *fluctuations* of $X_{\max}$ and $N_{\max}$. In figure 12 (13) $X_{\max}$ ($N_{\max}$) and its fluctuations are plotted as functions of the primary energy, for showers in the range 10^{14} – 10^{21} eV. It shows up clearly that: (i) The well-known proportionalities between $X_{\max}$ and $\log N_{\max}$ with and the logarithm of the primary energy [1, 17] do not hold exactly for electromagnetic showers of ultra-high energy when the LPM effect is taken into account. However, the mentioned linear relations are valid for proton showers in the whole range of energies considered. (ii) As mentioned, the fluctuations of $N_{\max}$ and especially those of $X_{\max}$ become larger as long

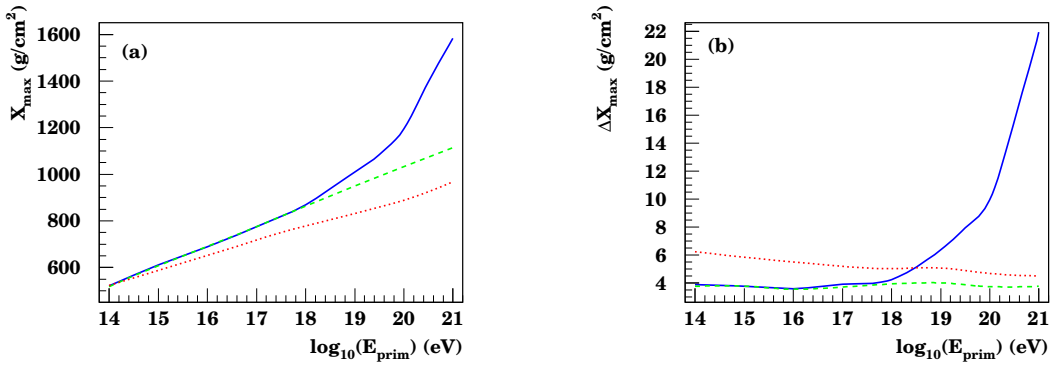

Figure 12. Computer simulation results for the shower maximum, $X_{\max}$, measured along the shower axis (a), and its fluctuations (RMS error of the mean) (b), plotted as function of the primary energy. The solid (dashed) lines correspond to gamma primaries taking (not taking) into account the LPM effect. The dotted lines correspond to proton primaries.

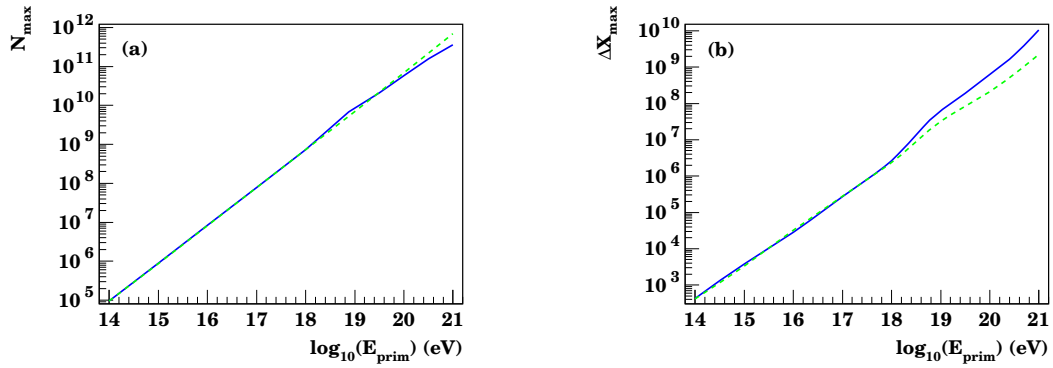

Figure 13. Number of charged particles at the shower maximum, $N_{\max}$, (a) and its fluctuations (RMS error of the mean) (b), plotted versus the primary energy. The primaries are gammas in the same conditions as in figure 12.

as the primary energy is increased, in comparison with the non-LPM counterparts. The results presented in this section correspond to particular cases which are representative of the behavior that should be expected in other general cases. Notice that the characteristics of electron initiated showers are very similar to those corresponding to gamma showers and the same remark can be done in the case of showers initiated by nuclei in comparison with proton showers. For that reason we are not including here any related plots.

5 Conclusions

We have analyzed exhaustively the LPM effect and the dielectric suppression from the theoretical point of view and have discussed the practical implementation of the corresponding algorithms for air shower simulations.

We have studied the different approaches to the LPM effect and conclude that the final results of the Migdal theory are best adapted for the numerical treatment while there are no important differences with the results coming from other approaches.

By means of numerical simulations using AIRES, we have studied the influence of the LPM effect, including dielectric suppression, on the longitudinal development of air showers initiated by ultra-high energy astroparticles. As mentioned previously, AIRES is capable of calculating many air shower observables in a realistic environment.

We have analyzed the influence of both suppression mechanisms for different primary particles in a wide range of energies. We have found that the LPM effect introduces significant modifications on the development of gamma and electron air showers if the primary energies are larger than 10^{19} eV. The most evident signature of the effect is the shift in the position of the maximum of the shower, which moves deeper into the atmosphere with increasing fluctuations when the primary energy is enlarged. Our conclusion is that in such cases the effect must be always taken into account in realistic simulations of ultra-high energy electromagnetic air showers. It is also important to remark that: (i) The influence of the dielectric suppression is not as important as the LPM effect, but large enough to have it taken into account in any realistic simulation. (ii) For shower with large zenith angles, the suppresion that delays the shower growth can be not as large as in the case of vertical showers, as explained in section 4.

We have not found any important effect in proton showers with primary energies up to 10^{21} eV. The reason for this, as explained in the previous section, is that the electromagnetic shower, where the LPM effect takes place, begins later, when the initial energy is shared among the secondary particles and the average energy per particle is then 2-3 orders of magnitude less than the primary energy. Clearly the same reasoning is valid for nuclei primary cosmic rays.

References

[1] T. K. Gaisser, *Cosmic Rays and Particle Physics,* Cambridge University Press (1992).

[2] H. Bethe and W. Heitler, *Proc. Roy. Soc.,* **A146**, 83 (1934).

[3] S. Klein, preprint hep-ph/9802442 (1998) (submitted to *Rev. Mod. Phys.*).

[4] L. D. Landau and I. J. Pomeranchuk, *Dokl. Akad. Nauk SSSR,* **92**, 535, 735 (1953). These papers are available in English in *The Collected Papers of L. D. Landau,* Pergamon Press (1965).

[5] A. B. Migdal, *Phys. Rev.,* **103**, 1811 (1956).

[6] M. L. Ter-Mikaelian, *"High Energy Electromagnetic Processes in Condensed Media"* Jon Wiley & Sons, New York (1972).

[7] P. Anthony *et al., Phys.Rev. D,* **56**, 1373 (1997).

[8] R. Blankenbecler and S. D. Drell, *Phys. Rev. D,* **55**, 190 (1997); *Phys. Rev. D,* **53**, 6285 (1996); SLAC report SLAC-PUB-95-6944 (1995).

[9] V. N. Baier and V. M. Katkov, *Phys. Rev. B,* **57**, 3146 (1998).

[10] B. G. Zackharov, preprint MPI-H-V44-1997 (to appear in *Sov. J. Nucl. Phys.*); *JETHP Lett.,* **64**, 781 (1996); *JETHP Lett.,* **63**, 952 (1996).

[11] R. Baier, Yu. L. Dokshitzer, A. H. Mueller and D. Schiff, *Nucl. Phys.,* **B478**, 577 (1996).

[12] J. Alvarez-Muñiz and E. Zas, preprint astro-ph/9806098; *Phys. Lett.,* **B411**, 218 (1997).

[13] S. J. Sciutto, *AIRES, a system for air shower simulations. User's manual and reference guide,* version 1.4.2 (1998). The AIRES software and documentation are available electronically at the following Web address: `www.fisica.unlp.edu.ar/auger/aires`.

[14] A. M. Hillas, *Nucl. Phys. B (Proc. Suppl.),* **52 B**, 29 (1997); *Proc. 19th ICRC (La Jolla),* **1**, 155 (1985).

[15] N. N. Kalmykov and S. S. Ostapchenko, *Yad. Fiz.,* **56**, 105 (1993); *Phys. At. Nucl.,* **56**, (3) 346 (1993); N. N. Kalmykov, S. S. Ostapchenko and A. I. Pavlov, *Bull. Russ. Acad. Sci. (Physics),* **58**, 1966 (1994).

[16] J. Engel, T. K. Gaisser, P. Lipari and T. Stanev, *Phys. Rev. D,* **46**, 5013 (1992).

[17] R. T. Fletcher, T. K. Gaisser, P. Lipari and T. Stanev, *Phys. Rev. D,* **50**, 5710 (1994).

[18] B. Rossi, *"High Energy Particles",* Prentice Hall (1956).

[19] R. C. Weast (editor), *CRC Handbook of Chemistry and Physics, 61st edition,* pp F206 – F213, CRC Press, Boca Raton (FL, USA) (1981).

[20] Y. S. Tsai, *Rev. Mod. Phys.,* **46**, 815 (1974).

[21] M. L. Perl, SLAC report SLAC-PUB-6514 (1994).

[22] W. H. Press, B. P. Flannery, S. A. Teukolsky and W. T. Vetterling, *Numerical Recipes, The Art of Scientific Computing*, Second edition, Cambridge University Press (1992).